

AD-A173 358

PHENOMENOLOGICAL STUDY OF THE BEHAVIOR OF SOME SILICA
FORMERS IN A HIGH V. (U) NATIONAL AERONAUTICS AND SPACE
ADMINISTRATION CLEVELAND OH LE. J D CAMLEY ET AL.

1/1

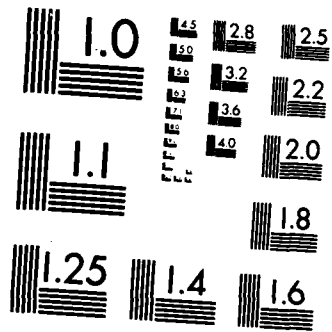
UNCLASSIFIED

OCT 85 NASA-E-2711 NASA-TN-87127

F/G 7/2

NL





MICROCOPY RESOLUTION TEST CHART
NATIONAL BUREAU OF STANDARDS-1963-A

2

NASA
Technical Memorandum 87127

USAAVSCOM
Technical Report 85-C-17

AD-A173 358

Phenomenological Study of the Behavior of Some Silica Formers in a High Velocity Jet Fuel Burner

James D. Cawley and Robert F. Handschuh
Propulsion Directorate
U.S. Army Aviation Research and Technology Activity—AVSCOM
Lewis Research Center
Cleveland, Ohio

DTIC
ELECTE
OCT 22 1985
S D

DTIC FILE COPY

October 1985

NASA

DISTRIBUTION STATEMENT A
Approved for public release;
Distribution Unlimited



86 10 21 009

PHENOMENOLOGICAL STUDY OF THE BEHAVIOR OF SOME SILICA FORMERS
IN A HIGH VELOCITY JET FUEL BURNER

J.D. Cawley and R.F. Handschuh
NASA Lewis Research Center and Propulsion Directorate
U.S. Army Aviation Research and Technology Activity - AVSCOM
Cleveland, Ohio 44135

SUMMARY

α
Samples of four silica formers: single crystal SiC, sintered α-SiC, reaction sintered Si₃N₄ and polycrystalline MoSi₂, were subjected to a Mach 1 jet fuel burner for 1 hr, at a sample temperature of 1375 °C (2500 °F). Two phenomena were identified which may be deleterious to a gas turbine application of these materials. The glass layer formed on the MoSi₂ deformed appreciably under the aerodynamic load. A scale developed on the samples of the other materials which consisted of particulate matter from the gas stream entrapped in a SiO₂ matrix.

INTRODUCTION

→ Silicon based materials are under consideration for a number of applications in aircraft and automotive gas turbine engines. The majority of these are monolithic components which benefit from the excellent high temperature strength of some of these materials, eg. sintered alpha silicon carbide and reaction bonded silicon nitride. Another possible application is employing these materials in turbine tip gas path seals. The structural requirement of this application is minimal, however dimensional stability is crucial.

The silicon based material are unstable in the presence of oxygen at the high temperatures experienced in the engine. Protection from gross reaction is afforded when an adherent film of SiO₂ forms on the surface during oxidation. This film serves as a barrier across which mass transport must occur for further oxidation, leading to parabolic scale growth kinetics. The class of materials which displays this behavior is termed silica formers.

It has been postulated that one-dimensional growth of an oxide film with a positive volume change, and parabolic kinetics on the surface of a turbine tip seal can be favorable (ref. 1). An additional requirement for this is that the oxide film is not deformable under the frictional forces produced by gas flow through the engine.

The materials studied were; molybdenum disilicide, single crystal silicon carbide, sintered alpha silicon carbide, and reaction bonded silicon nitride. It is well documented (e.g. ref. 2) that under a static air environment, at temperatures in excess of 1500 °C (2730 °F), these materials oxidize to produce an adherent scale of vitreous silica. The purpose of this work was to examine the morphology of scales produced when oxidation took place in the high velocity effluent of a (Mach 1) jet fuel burner.



Codes	
Dist	Avail and/or Special
A-1	

E-2711

EXPERIMENTAL

The sample sources, geometries, and surface preparations are detailed in table I.

The burner rig used was the NASA Lewis High Temperature Erosion Rig which is described in detail in reference 3. The essential components of the rig are a jet fuel combustor, a Mach 1 nozzle, and a sample holder, see figure 1. The rig also has provision for introducing grit particles to the gas stream, however this was not used.

The samples were placed in sample holder 50 mm (2 inch) from the nozzle exit slightly inclined, 15°, from perpendicular. Temperatures were measured using pyrometers. The same rig parameters (fuel pressure, air pressure, etc.) were used in all cases. Some variation was found in the temperature measurements with readings between 1325 and 1390 °C (2420 and 2535 °F). The diameter of the flame on the sample was 8 mm, (0.3 inch) outside of this a steep thermal gradient existed. Sighting of the pyrometer may have contributed to the scatter. The time of exposure to the flame was 1 hour in all cases.

RESULTS

Molybdenum Disilicide

Two types of surface preparation were used on the MoSi₂ rods: as ground and static preoxidation at 1300 °C (2340 °F) for 24 hr. Both types were run in the Mach 1 burner rig for 1 hr at 1375 °C (2510 °F). The post test condition of the rods is shown in figures 2 and 3. From these photographs it is apparent that the SiO₂ produced through oxidation was physically blown from the leading edge and accumulated on the leeward side of the rod. This leaves the MoSi₂ unprotected and allows the reaction to proceed as evidenced by the extensive pitting on the rod surface. The sample given the static oxidation appears to have less severe corrosion than the as-ground sample, however it is clear from the photographs that the preoxidation did not affect the character of the reaction.

Single Crystal Silicon Carbide

The single crystal silicon carbide was exposed to the burner in an as-polished state. The behavior was qualitatively different from that of the MoSi₂. Scaling, or a buildup of material on the SiC surface occurred directly under the location of the flame, see figure 4, while the rest of the surface displayed interference colors typical of passive oxidation. A typical cross section of the scale material is shown in figure 5. The thickness (50-100 μm) is far in excess of what is expected from the formation of SiO₂ during passive oxidation (≈0.2 μm) for 1 hr at 1375 °C (2510 °F).

Two sources of unanticipated sources of particulates were identified after the experiments were run. The first was residual alumina grit particles from previous operation of the rig in the erosion mode. Evidently a certain fraction of the grit particles which had accumulated in the plumbing of the rig became entrained in the gas stream during our experiments. It should be noted that no erosion due to particle impact has been observed for either oxide or

metal specimens under these conditions. This implies that the number density of these residual particles is small.

The second source of particulates was the sample holder itself. As illustrated in figure 11, the stainless steel clamping block used to hold the specimen had a corner which protruded very close to the main gas stream. Some erosion of metal from this corner was observed. These erosion products would be expected to become entrained in the gas stream.

The microstructure of the scale is complex. There is an intermittent contact between the scale and the carbide. The scale also appears cracked and contains inclusions. Energy dispersive x-ray analysis revealed the presence of Si, Al, Fe, and Ti. Using an electron microprobe, element mapping was done near the carbide/scale interface. Maps for Si, Al, Fe, and O are shown in figures 4 to 7 respectively. It is clear from these that silicon and aluminum are present as oxides while iron is present as a metallic species. A second, and striking, feature is that the silica phase is the minority phase by volume but it forms a continuous matrix which contains inclusions of alumina and iron. Reference to the micrographs also indicates that the scale thickness is several times the diameter of the inclusions. These micrographs therefore suggest a mechanism for scale growth by the adhesion of particles in a "glue" of silica. This can give rise to the formation of scales which are many times thicker than what is predicted on the basis of oxidation alone.

Sintered Alpha Silicon Carbide

Samples of both as-fabricated and as-fabricated plus static oxidation at 1300 °C (2370 °F) for 24 hr were exposed to the burner. The preoxidation had no effect on the observed result. The scale growth on the sintered alpha silicon carbide appeared qualitatively the same as the single crystal silicon carbide except that the boundary of the scaled region is less distinct, see figure 12. Attempts at a transverse section were unsuccessful.

It was also observed, under high magnification, that the scale contained a high density of bubbles, see figure 13, which is typical for this material (ref. 4).

Reaction Bonded Silicon Nitride

One sample of silicon nitride in as-fabricated form was exposed to the burner. A scale formed on the block which visually appeared to be similar to that formed on the silicon carbide. It was not investigated on the microscopic level.

DISCUSSION

Identification has been made of two phenomena which may affect the suitability of the use of silica formers in gas turbines. The first was the deformation of the oxide scale film under the aerodynamic load. This is highly undesirable because the existence of a continuous mass transport barrier is fundamental to passive behavior. It is notable that the SiO_2 film on the MoSi_2 was observed to be much more deformable, inferentially of a lower viscosity,

than that on the silicon carbide. The reason for this is unclear, it is possible to speculate that the presence of molybdenum reducing the viscosity of the scale.

In the appendix a simple model is developed to determine the deformation and mass flow of a viscous glass film due to aerodynamic friction over an oxidized rod. The model was applied using molybdenum disilicide parabolic rate constants (ref. 5) at various stagnation point (on the rod) oxide layer thicknesses and viscosities. The model results are shown in figure 14. The observed mass flow suggests a viscosity several orders of magnitude lower than that reported for vitreous silica at this temperature (viscosity $\approx 1.0 \times 10^9$ N·s/m² at 1450 °C).

The severity of this problem might also be enhanced during long time exposures when impurities in the fuels (such as Ca, Cu, Fe, and Pb) may deposit on and reduce the viscosity of the scale.

The second phenomenon observed was the adhesion of debris within a matrix of SiO₂ somewhat analogous to bricks and mortar. The SiO₂ was not the major phase by volume but served the role as the binder. This would be a problem in a seal application if debris collects on the seal surface producing high spots that lead to rubs against the turbine blades. It would also be undesirable to have the shape and surface roughness of airfoils made from silica formers modified by the deposition and adherence of debris. While the types of debris observed were particular to the test set up it is anticipated that any type of particulate ingested or produced in an engine would likely adhere.

CONCLUSIONS

These experiments were somewhat preliminary in nature and further experimentation under more controlled circumstances is desired, however, it may be concluded that:

1. The SiO₂ film formed on the MoSi₂ rods deformed appreciably under the aerodynamic load of the high velocity effluent of a Mach 1 jet fuel burner.
2. The scale formed on single crystal silicon carbide was composed of metal and oxide particulates embedded in matrix of SiO₂. These scales were several particle diameters thick and many times thicker than expected from oxidation alone.
3. The scales formed on sintered alpha silicon carbide and reaction bonded silicon nitrides appeared similar to the scale formed on the single crystal silicon carbide.

APPENDIX: EFFECT OF HIGH TEMPERATURE COMBUSTION FLOW OVER
AN OXIDIZED ROD

A simple flow model is developed to determine the deformation of a viscous glass film due to aerodynamic friction at high temperatures as a function of position on the periphery of the oxidized rod. The overall model is shown in figure (15) with the parameters of interest indicated.

The assumptions used for this analysis are as follows:

- (1) constant gas temperature equal to 1700 K.
- (2) Constant gas velocity equal to sonic velocity for air at 1700 K.
- (3) Linear pressure drop (constant pressure gradient) around the periphery from the stagnation point to the separation point (ref. 6). Pressure was assumed to be the same in the highly viscous layer as in the gas.
- (4) Shear stress due to the hot gas acting on the oxide layer was constant and was found from a potential flow solution to the Navier-Stokes equations for cylindrical geometry (ref. 7).
- (5) The rate constant for oxide layer growth was assumed to be constant and given in reference 8.

Analysis

First the continuity equation is applied to the model and is shown in figure 16. The change in mass flow, $\Delta\dot{m}$, is given by the following equation:

$$\Delta\dot{m} = (R\Delta\theta)(\Delta Z) \rho\dot{M} \quad (A1)$$

where

R radius of the rod

$\Delta\theta$ angular increment

ΔZ depth (length) of rod

ρ density of viscous layer (oxide)

\dot{M} rate of flow of rod material to oxide layer

The mass flow rate, \dot{M} , of the rod to oxide layer is given by

$$\dot{M} = \frac{\tilde{K}_p}{\delta} = \frac{K_p}{\delta\rho^2} \quad (A2)$$

K_p parabolic rate constant from reference A3

δ viscous layer thickness

The rate constant K_p was taken from reference 8 and its value used in this analysis was

$$K_p = 4.8 \times 10^{-7} \frac{\text{Kg}^2}{\text{m}^4 \cdot \text{s}}$$

which was the experimental value found in reference 8 for molybdenum disilicide at 1645 K and partial pressure of oxygen of 14 torr.

Substituting equation (A2) into (A1) gives:

$$\left(\frac{1}{\Delta Z}\right) \left(\frac{\Delta \dot{m}}{\Delta \theta}\right) = R \rho \left(\frac{\tilde{K}_p}{\delta}\right) \quad (\text{A3})$$

Letting $\bar{\Delta \dot{m}}$ be the change in mass flow rate unit depth and letting $\Delta \theta$ approach zero gives:

$$\frac{d\bar{\dot{m}}}{d\theta} = R \rho \left(\frac{\tilde{K}_p}{\delta}\right) \quad (\text{A4})$$

This expression determines the rate of flow of rod material with respect to angular position and is dependent on the oxide layer thickness.

Next the momentum equation is needed to determine the loading effect on the oxide layer thickness. Figure 17 shows the model used for this formulation.

The forces that are on the oxide layer are shown in figure 17. For a nondeformable control volume in steady flow the sum of the forces is given by (ref. 6):

$$\sum F = \int_{\text{C.S.}} \rho V(V \cdot \hat{n}) dA \quad (\text{A5})$$

For low Reynolds number flow the flux terms on the right hand side of equation (A5) can be neglected. From the diagram this gives

$$- (\Delta P \delta L) + \tau_0 (R \Delta \theta) L = \tau R L \Delta \theta \quad (\text{A6})$$

or:

$$- (\Delta P \delta) + \tau_0 (R \Delta \theta) = \tau R \Delta \theta \quad (\text{A7})$$

Dividing through by $\Delta \theta$

$$- \left(\frac{\Delta P}{\Delta \theta}\right) \delta + \tau_0 R = \tau R \quad (\text{A8})$$

where

$\frac{\Delta P}{\Delta \theta}$ pressure gradient

τ_0, τ shear stress gas to oxide, oxide to rod

The gas pressure was assumed to decrease linearly as a function of θ , from the stagnation point to the separation point (fig. 15). The pressure was assumed to behave by Bernoulli's Theorem given by reference 6 as:

$$P_1 + \frac{1}{2} \rho V_1^2 = C_1 \quad (A9)$$

which means the total pressure is constant or

$$P_1(\theta_1) = C_1 - C_2 \theta_1$$

$$\frac{\Delta P_1}{\Delta \theta_1} = - C_2 \quad (A9a)$$

where P_1, V_1 pressure and velocity at position θ_1 .

The constants, C_1 and C_2 were found by using the property data of Jet A fuel burned in air found in reference 9, and the assumed sonic velocity of the high temperature gas. For this analysis C_1 and C_2 were found from

$$\rho = 0.2122 \text{ Kg/m}^3,$$

$$V = 826 \text{ m/s, and}$$

$$P = 1.0133 \times 10^5 \text{ N/m}^2;$$

$$C_1 = 1.737 \times 10^5 \text{ N/m}^2$$

$$C_2 = 3.7878 \times 10^4 \text{ N/(m}^2 \cdot \text{radian)}$$

The next parameter needed in equation (A8) was, τ_0 , or the shear stress acting on the gas-oxide surface. An integrated average value was found from figure 18. This figure plots the nondimensional shear stress versus nondimensional position for various types of bodies. These curves were developed from a potential flow solution of the Navier-Stokes equations (ref. 7) for various shaped bodies. Using the parabolic shape of the circular cylinder plot an integrated average nondimensional shear stress was found. This value, $\overline{\tau}_0$, was found to be equal to 4.066. This value along with the gas properties provided the average shear stress τ_0 .

$$\overline{\tau}_0 = \frac{2\tau_0}{\rho U_\infty^2} \sqrt{\frac{U_\infty d}{\nu}} \quad (A10)$$

U_∞ free stream gas velocity; ($U_\infty = V_{sep}$)

ρ gas density

ν kinematic viscosity of the gas

d diameter of the rod

Solving for τ_0 with the appropriate values gives: $\tau_0 = 2106.7 \text{ N/m}^2$ per unit depth.

To evaluate the shear stress between the viscous oxide layer and the rod, τ , it is necessary to evaluate the flow of the oxide layer first.

$$\dot{m}_i = \rho \delta_i L \bar{V}_\theta \quad (\text{A11})$$

\dot{m}_i mass flow rate of oxide layer at i^{th} position

ρ density of viscous layer

δ_i oxide layer thickness at position i

L length of rod exposed to gas flow

\bar{V}_θ average velocity across oxide layer thickness

If it is assumed that the velocity profile in the oxide is parabolic, then the velocity as a function of position in the oxide is given by:

$$V_\theta(y) = A + By + Cy^2 \quad (\text{A12})$$

where y is the coordinate in the normal direction from the rod surface. The following boundary conditions are imposed:

Boundary Condition 1: $V_\theta = 0$ at $y = 0$ (at the rod-oxide interface)

Boundary Condition 2: $\frac{\partial V_\theta}{\partial y} = 0$ at $y = \delta$

Using condition (1) in equation (A12) gives

$$A = 0$$

using condition (2) in equation (A12) gives:

$$B = -2 C \delta$$

Substituting A and B into equation (A12)

$$V_\theta(y) = -2C\delta y + Cy^2 \quad (\text{A13})$$

For the continuity equation the average velocity, \bar{V}_θ , is needed and this is given by reference 6 to be:

$$\bar{V}_\theta(y) = \frac{1}{\delta} \int_0^\delta V_\theta dy \quad (\text{A14})$$

Substituting equation (A13) into (A14) and evaluating gives the following expression for average velocity:

$$\bar{V}_\theta = -\frac{2}{3} C \delta^2 \quad (\text{A15})$$

inserting equation (A15) into equation (A11) and solving for C gives:

$$C = -\frac{3\bar{m}}{2\rho\delta^3} \quad (\text{A16})$$

Now using equation (A13) and the relationship between shear stress and velocity profile:

$$\tau = \mu \left. \frac{\partial V_\theta}{\partial y} \right|_{y=0} \quad (\text{shear stress at the interface}) \quad (\text{A17})$$

$$\left. \frac{\partial V_\theta}{\partial y} \right|_{y=0} = -2C\delta \quad (\text{A18})$$

Substituting equation (A18) into (A17) the shear stress at the oxide-rod interface is:

$$\tau = \frac{3\mu\bar{m}}{\rho\delta^2} \quad (\text{A19})$$

μ oxide layer viscosity

\bar{m} flow rate of oxide per unit length

ρ oxide layer density

δ oxide layer thickness

Now the shear stress between the rod and the oxide layer is known in terms of the oxide layer flow rate and the oxide layer thickness. Now equations (A19), (A10), and (A9a) can be inserted into equation (A8) and solved for " δ ", the oxide layer thickness. This equation then becomes:

$$\delta^3 + \frac{\tau_0 R}{\left(\frac{\Delta P}{\Delta \theta}\right)} \delta^2 - \frac{3\bar{m}\mu R}{\rho \left(\frac{\Delta P}{\Delta \theta}\right)} = 0 \quad (\text{A20})$$

Numerical Method

The numerical model used is shown in figure 19. The procedure used is as follows:

- (1) Assume an initial layer thickness δ_0 at the first step, set $\bar{m}_0 = 0$.

- (2) Use the initial guess δ_0 with equation (A4) and a fourth-order Runge-Kutta approximation to find the mass flow rate per unit depth \bar{m}_1 at the 1th position.
- (3) Using \bar{m}_1 just found, substitute into equation (A20). Note:

$$\left(\bar{m}_{1+1} = \bar{m}_1 + d\bar{m}/d\theta_1 \Big|_{\delta_1} \right)$$
- (4) Solving the third degree equation by Newton's Method for δ_{1+1} .
- (5) This is now used at the next position for \bar{m} in equation (A4).
- (6) Repeat the process until the separation point is reached.

Numerical Results

The numerical results of the above analysis are shown on figure 14 as presented in the discussion. This figure is a summary of varying the initial layer thickness δ_0 and the oxide layer viscosity on the mass flow rate per unit depth at the separation point. At high viscosity the behavior of the mass flow is dominated by the oxide thickness, δ_0 , at the stagnation point. However, as the oxide layer viscosity decreases the effect of a thin initial layer is minimal on the mass flow rate at the separation point on the rod. This is evident as the plotted mass flow rate per unit depth is invariant for two orders of magnitude difference in the initial oxide layer, δ_0 , thickness.

REFERENCES

1. Cawley, J.D.: Oxidizing Seal For the Turbine Tip Gas Path. U.S. Patent Application SN-602050, Apr. 19, 1984.
2. Schlichting, Jurgen: Oxygen Transport Through Silica Surface Layers on Silicon Containing Materials. High Temp. High Press., vol. 14, no. 6, 1982, pp. 717-724.
3. Handschuh, R.F.: High Temperature Erosion of Plasma-Sprayed Yttria-Stabilized Zirconia in a Simulated Turbine Environment. NASA TP-2406, 1984.
4. Mieskowski, D.M.; Mitchell, T.E.; and Heuer, A.H.: Bubble Formation in Oxide Scales on SiC. J. Am. Ceram. Soc., vol. 67, no. 1, Jan. 1984, pp. C17, Jan. (1984).
5. Chang, Y.A.: Oxidation of Molybdenum Disilicide. J. Mater. Sci., vol. 4, no. 7, July 1969, pp. 641-643.
6. Potter, M.C.; and Foss, J.F.: Fluid Mechanics. Ronald Press Co., New York, 1975.
7. Streeter, V.L.: Handbook of Fluid Dynamics. McGraw-Hill, 1961.
8. Chang, Y.A.: Oxidation of Molybdenum Disilicide. J. Mater. Sci., vol. 4, no. 7, July 1969, pp. 641-643.
9. Poferl, D.J.; Svehla, R.A.; and Lewandowski, K.: Thermodynamics and Transport Properties of Air and the Combustion Products of Natural Gas and of ASTM-A-1 Fuel With Air. NASA TN-D-5452, 1969.

TABLE I. - SPECIMEN TYPE, SOURCE, AND GEOMETRY

Sample I.D.	Source	Burner rig sample geometry
^a Molybdenum disilicide (2 specimen)	Kanthal Corp.	rods, 5 mm (0.2 inch) diameter
^b Single crystal silicon carbide	Carborundum Co., Acheson furnace ^c	crystals, roughly 10x10x3 mm (0.4x0.4x0.12 inch)
^d Sintered alpha silicon carbide (2 specimen)	Carborundum Co. ^c	quarters of a tube, 18 mm (0.7 inch) o.d.
^e Reaction bonded silicon nitride	Air Research Casting Co.	blocks, 13x25x50 mm (0.5x1x2 inch)

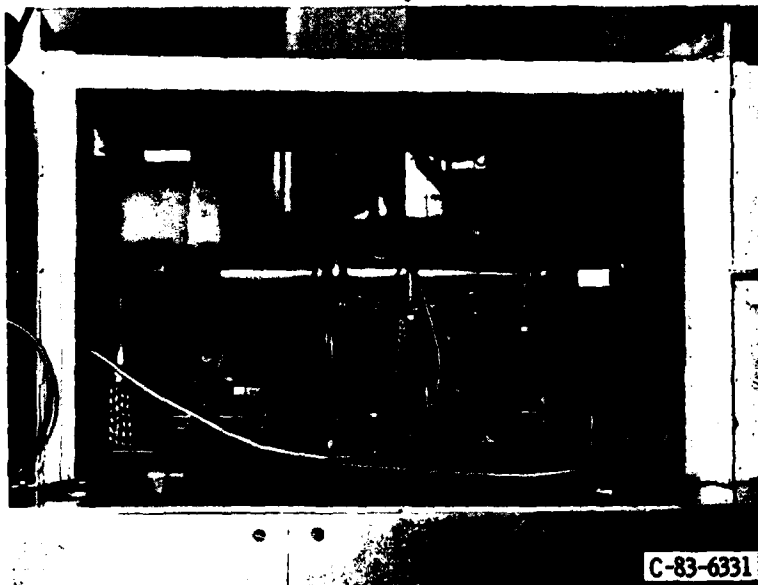
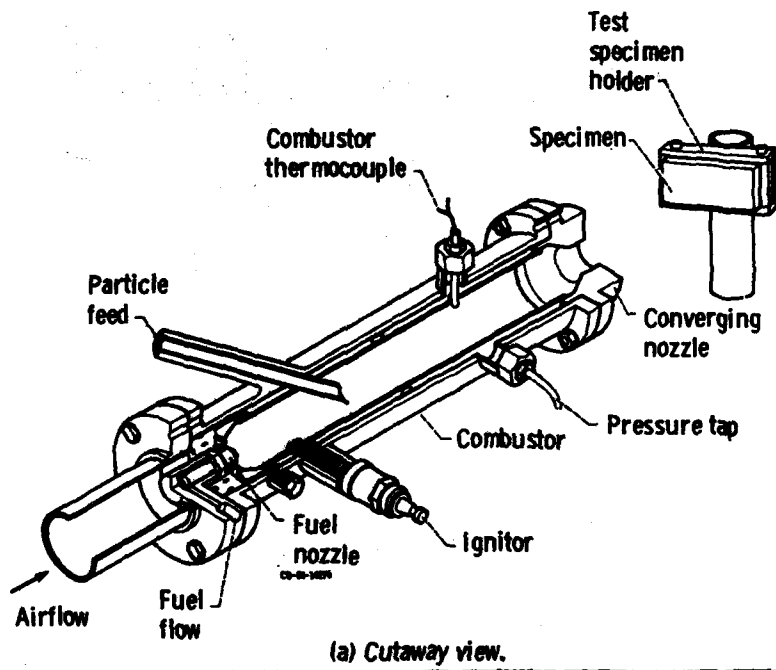
^aSurface preparation: First specimen etched with HF (25%) for 45 min, finished ground with 325 mech SiC. Second specimen same as first then statically oxidized in air at 1300 °C (2370 °F) for 24 hr.

^bSurface preparation polished to scratch free surface with successive grades of diamond paste down to 1/4 μm.

^cSupplied by J.W. Halloran Case Western Reserve University.

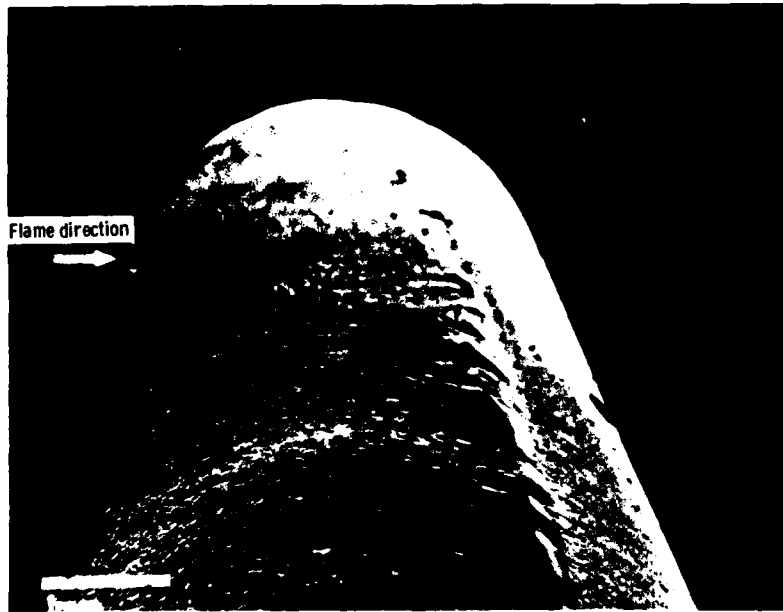
^dSurface preparation: first specimen as fabricated, second specimen statically oxidized in air at 1300 °C (2370 °F) for 24 hr.

^eSurface preparation; as fabricated.



(b) Test installation.

Figure 1. - High-temperature erosion rig.



(a) Axis of MoSi₂ rod.



(b) SEM micrograph close up of the SiO₂ ridge.

Figure 2. - SEM micrograph of a MoSi₂ rod which was statically oxidized for 24 hr at 1300 °C then oxidized in the Mach 1 burner rig at 1375 °C for 1 hr.



Figure 3. - SEM micrograph along the axis of a MoSi₂ rod which was ground with 320 mesh SiC and oxidized in the Mach 1 burner rig at 1375 °C for 1 hr.

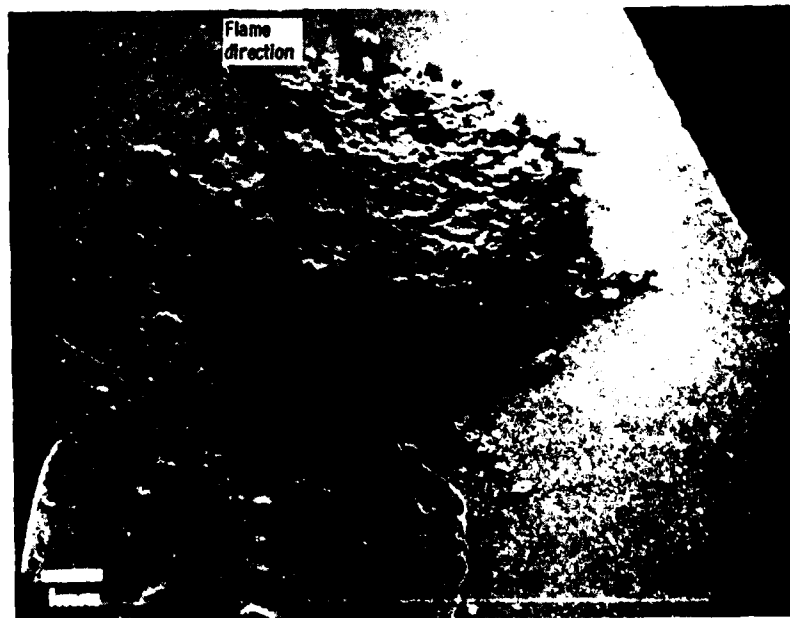


Figure 4. - SEM micrograph of single crystal SiC surface after 1 hr oxidation at 1375 °C in the Mach 1 burner rig.



Figure 5. - SEM micrograph of the cross section of the builtup material using backscattered electrons.

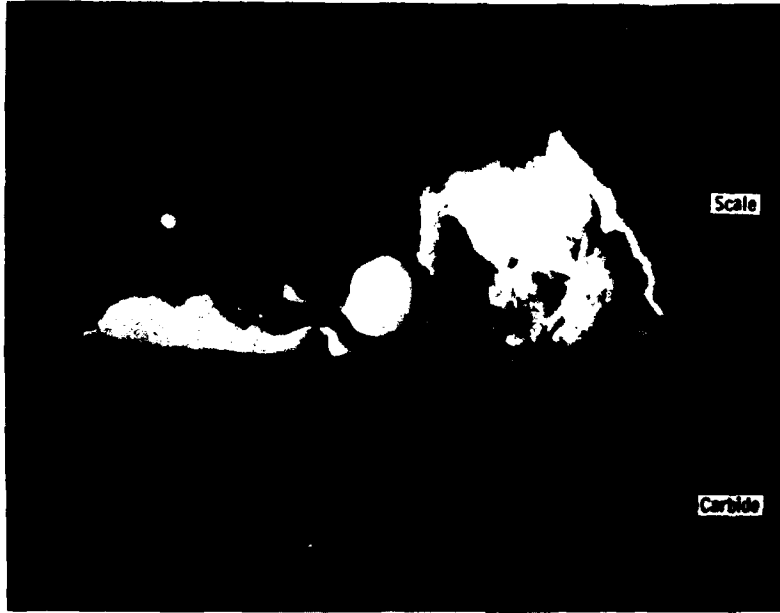


Figure 6. - Electron microprobe image of carbide/scale interface using backscattered electrons.

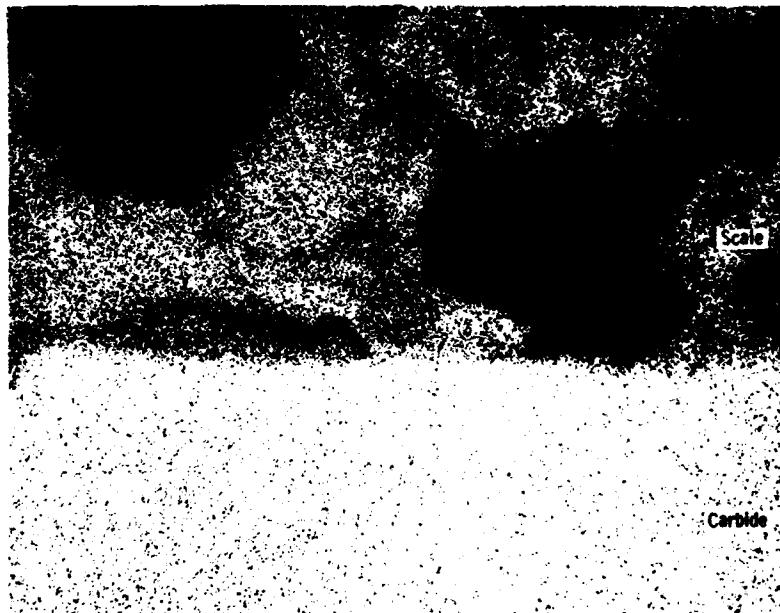


Figure 7. - Silicon elemental distribution around carbide/scale interface.



Figure 8. - Aluminum elemental distribution around carbide/scale interface.

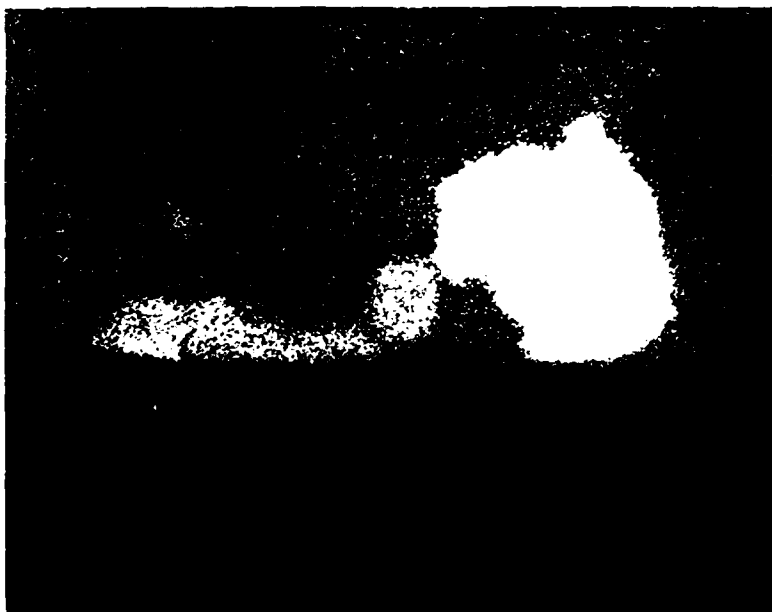


Figure 9. Iron elemental distribution around carbide/scale interface.



Figure 10. - Oxygen elemental distribution around carbide/scale interface.

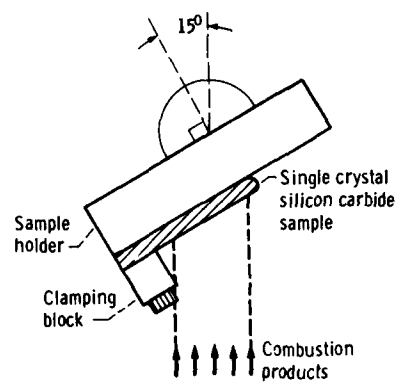


Figure 11. - Specimen holding fixture showing the orientation of test hardware in the jet fuel combustion products.



Figure 12. - SEM micrograph of the scale built up on the sintered alpha silicon carbide.

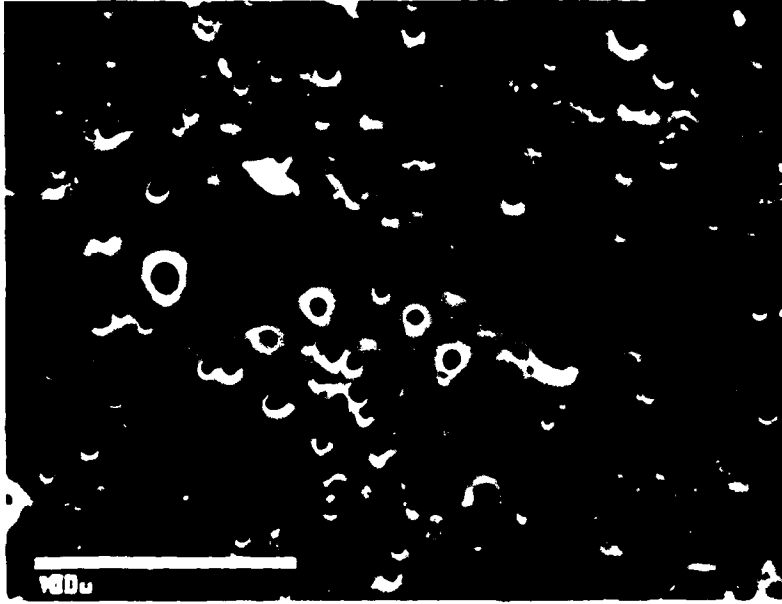


Figure 13. - High magnification SEM micrograph of the scale formed on sintered alpha silicon carbide.

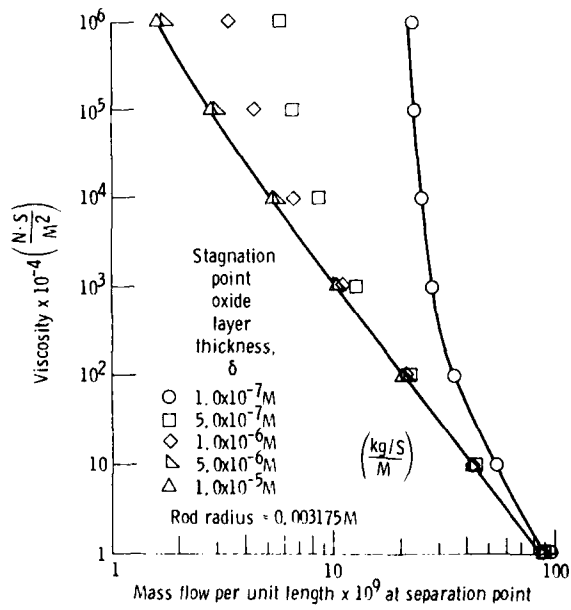


Figure 14. - Effect of initial layer thickness on mass flow per unit depth at the separation point for a wide range of viscosity of oxide layer. (M_0Si_2 rod).

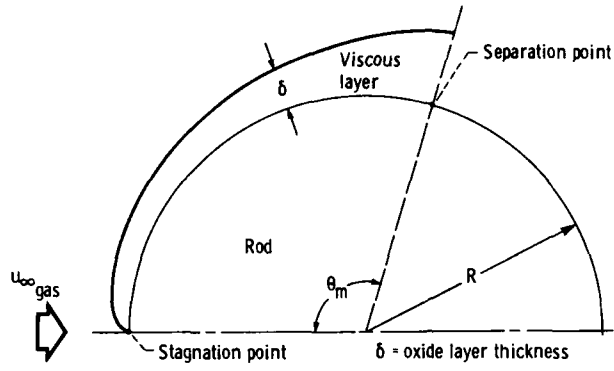


Figure 15. - Model of system analyzed.

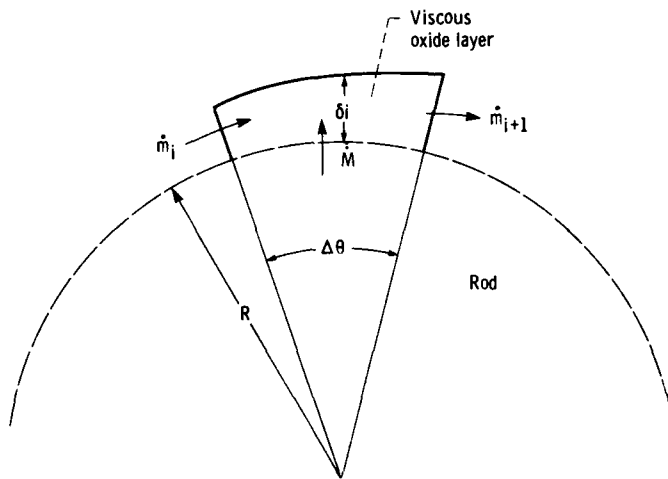


Figure 16. - Continuity equation model.

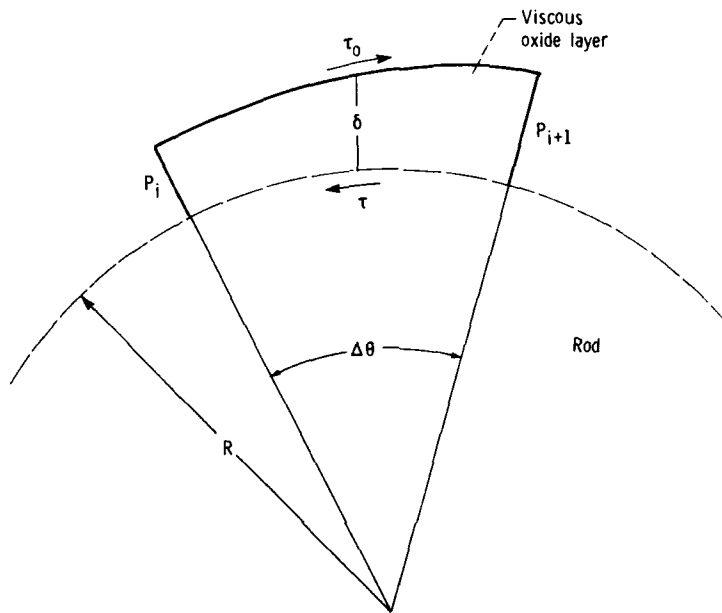


Figure 17. - Momentum equation model.

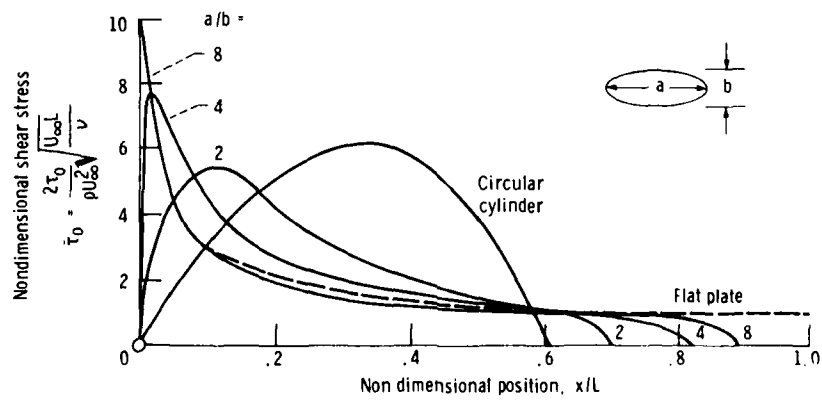


Figure 18. - Shear stress as a function of position for various geometry. From Fluid Dynamics Handbook by Streeter. For circular cylinder: $X = \theta_1$; $L = \theta_m$ at $X/L = .609$ separation point a/b - aspect ratio for elliptic bodies.

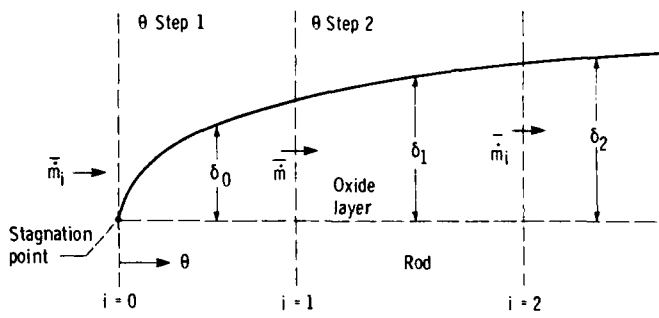


Figure 19. - Numerical model.

1. Report No. NASA TM-87127 USAAVSCOM-TR-85-C-17		2. Government Accession No. ADA173358		3. Recipient's Catalog No.	
4. Title and Subtitle Phenomenological Study of the Behavior of Some Silica Formers in a High Velocity Jet Fuel Burner				5. Report Date October 1985	
				6. Performing Organization Code 505-33-7B	
7. Author(s) J.D. Cawley and R.F. Handschuh				8. Performing Organization Report No. E-2711	
				10. Work Unit No.	
9. Performing Organization Name and Address NASA Lewis Research Center and Propulsion Directorate, U.S. Army Aviation Research and Technology Activity- AVSCOM, Cleveland, Ohio 44135				11. Contract or Grant No.	
				13. Type of Report and Period Covered Technical Memorandum	
12. Sponsoring Agency Name and Address National Aeronautics and Space Administration Washington, D.C. 20546 and U.S. Army Aviation Systems Command, St. Louis, Mo. 63120				14. Sponsoring Agency Code	
				15. Supplementary Notes	
16. Abstract <p>Samples of four silica formers: single crystal SiC, sintered α-SiC, reaction sintered Si₃N₄ and polycrystalline MoSi₂, were subjected to a Mach 1 jet fuel burner for 1 hr, at a sample temperature of 1375 °C (2500 °F). Two phenomena were identified which may be deleterious to a gas turbine application of these materials. The glass layer formed on the MoSi₂ deformed appreciably under the aerodynamic load. A scale developed on the samples of the other materials which consisted of particular matter from the gas stream entrapped in a SiO₂ matrix.</p>					
17. Key Words (Suggested by Author(s)) Silicon-based material; Oxidation; Silica former; Gas turbine			18. Distribution Statement Unclassified - unlimited STAR Category 37		
19. Security Classif (of this report) Unclassified		20. Security Classif (of this page) Unclassified		21. No of pages	22. Price* A02

END

12-86

DTIC